

NUMERICAL SIMULATION OF HELIUM DISPERSION IN A SEMI-CONFINED AIR-FILLED CAVITY

Huong-Lan Tran^{1,2}, Anne Sergent^{1,3}, Gilles Bernard-Michel², Patrick Le Quere¹

¹ *LIMSI-CNRS, UPR 3251, 91403 Orsay cedex,
e-mail : huonglan@limsi.fr*

² *D.E.N, D.A.N.S, S.E.M.T,
L.T.M.F, Bât. 454, CEA Saclay,
Gif-Sur-Yvette, France*

³ *UPMC Paris 06, 75005 Paris*

ABSTRACT

This paper deals with the build-up of concentration when a continuous source of helium is supplied in an air-filled enclosure. Our aim is to reproduce the results of a small-scale experimental study ([11]). To begin with, the size of the experiment is reduced from 1/10 to 3/5 for the present analysis. Hypotheses are made in order to reduce the dimension of the real problem. Numerical simulations are carried out on fine grids without any turbulence modeling. The flow structure and the concentration profile of the resulting flow are analyzed and compared with theoretical results.

NOMENCLATURE

D	Helium diffusivity in air [$\text{m}^2.\text{s}^{-1}$]	α	Entrainment coefficient
\mathbf{g}	Gravity acceleration vector [$\text{m}.\text{s}^{-2}$]	ϵ_M	Molar mass fraction of air to helium
Gr	Grashof number	ν	Kinematic viscosity[Pa.s]
H	Cavity height [m]	ρ	Mixture density [$\text{kg}.\text{m}^{-3}$]
L	Cavity depth [m]	B_0	Source buoyancy flux [$\text{m}^2.\text{s}^{-1}$]
p	Pressure [Pa]	d_i	Nozzle diameter[m]
r	Radial coordinate [m]	Q_0	Injection flow rate [$\text{m}^3.\text{s}^{-1}$]
Sc	Schmidt number	Ri_0	Injection Richardson number
\mathbf{u}	Mixture velocity [$\text{m}.\text{s}^{-1}$]	Ri_v	Volume Richardson number
V	Volume of enclosure [m^3]	U_0	Average injection velocity [m^2]
W	Cavity width [m]	X	Helium volume fraction
z	Vertical coordinate [m]	Y	Helium mass fraction

I. INTRODUCTION

The new generation of cars using hydrogen as an energy carrier is a promising replacement for traditional cars using gasoline, which cause CO₂ emission. Safety study on the dispersion mechanism of hydrogen in air has to be done carefully before they come into widespread use. A typical accidental situation is when there is a leak in a confined environment, such as a garage or a fuel cell, in which the concentration build-up may lead to hazardous consequences. Such problems of buoyant convection from an isolated source in a confined environment are classical and have been widely studied in the literature ([2]-[11]).

When a continuous source of fluid is supplied in an enclosure, the ambient fluid is gradually contaminated and its concentration is modified. This raises the question of how to predict precisely the concentration distribution at a given time. It is well-known that the resulting flow depends on both the characteristics of the source and the environment in which the flow develops. Depending on the injection Richardson number the source flow can be dominated either by buoyancy or inertia [1]. For buoyancy-dominated flows, Baines and Turner [2] developed a theoretical model for the filling process in an enclosure. This process produces a stable vertical density stratification from the initial homogeneous ambient. The buoyant fluid arriving at the top wall with small enough momentum spreads out horizontally and forms a thin layer. This layer is separated from the ambient fluid below it by what called the first front. The solutions were given for the velocity of this front before it arrives at the bottom and the density profile of the environment at long time. The most important physical assumption is that the entrainment into the plume is proportional to the local mean upward velocity in the plume. It is also supposed that the produced plume has an axisymmetric mean profile and the area containing plumes is a small fraction of the total area at any level. Their model has been verified by an experiment with salt-water solution where the entrainment coefficient was taken equal to 0.1. Later, Worster and Hupper [3] extended this model to predict the density profile of the environment during the descent of the first front. At long times, this model tends to the model of Baines and Turner [2]. The geometrical condition for which the analyses of [2] and [3] are valid is that the ratio height-to-horizontal diameter of the cavity H/d does not exceed 0.5.

For more general situations of the source and the enclosure, the models of [2] and [3] do not always apply. Cleaver et al. [6] carried out both small-scale and large-scale experiments on buoyant jets of natural gas and proposed a criterion to predict the build-up of concentration in an enclosed cavity, in terms of a volume Richardson number. For high values of this number compared to unity, overturning does not occur and a stable stratification is predicted by the models of [2] and [3]. Otherwise, overturning occurs and the fluid near the ceiling is mixed to produce a homogeneous layer. An empirical formula for the thickness of this homogeneous layer was also given. In order to determine the limit of this homogeneous layer, Cariteau [4] conducted a set of experiments with helium-air mixture and helium in a confined volume with various source conditions. Three filling regimes: stratified, stratified with homogeneous layer and homogeneous have been identified depending on the volume Richardson number. Although this experiment does not satisfy the condition $H/d \leq 0.5$ of Baines and Turner's model [2], the experimental results in the stratified regime were found consistent with this model. However, the results for a smaller source contradicts this model. In this experiment, helium is often used as a model gas for hydrogen to avoid explosion risk and the appropriateness of this alternative has been justified in [10].

Numerical modeling is a powerful tool in safety study which gives access to a wide range of param-

eters and geometry. For validation purposes, experiments in simplified configuration are carried out to give reference data and elementary test cases. A benchmark based on the experiment of [4] has been proposed to test numerical models [11]. Participants used either turbulence models or subgrid-scale models and their numerical results are different from the experimental data. The maximum concentration is either underestimated or overestimated by at least 25 %. The minimum concentration is highly overestimated by all the teams. It has been shown that the low injection case is a challenge for numerical modeling.

In this paper we deal with the build-up of concentration when a continuous source of helium is supplied to an air-filled enclosure. Our purpose is to reproduce the results of the benchmark [11] using Direct Numerical Simulation (DNS). To begin with, the size of the experiment is reduced for the present analysis. Hypotheses are made in order to reduce the dimension of the real problem. The structure of the resulting flow is investigated. The concentration profile is compared to the theoretical model of [3] and the experimental results of [11].

The paper is organized in four parts. Firstly, we give a short background summary on the subject. Then the problem model and numerical methods used in our simulations are introduced. Two last sections are devoted to numerical results and the discussion of those results.

II. BUOYANT CONVECTION FROM AN ISOLATED SOURCE IN A CONFINED ENVIRONMENT

The resulting flow of buoyant convection from an isolated source in a confined environment depends on both the characteristics of the source and the environment in which the flow develops. The source is characterized by an injection Richardson number defined by

$$Ri_0 = \frac{1}{2} g \frac{\rho_a - \rho_i}{\rho_i} \frac{d_i}{U_0^2} \quad (1)$$

where g is the gravitational acceleration, ρ_a and ρ_i is the density of the ambient and injected fluid, respectively, U_0 is the average speed at the source and d_i is the diameter of the source. If $Ri_0 \gg 1$ the source flow is dominated by buoyancy and if $Ri_0 \ll 1$ the source flow is dominated by inertia.

When the source flow is dominated by buoyancy and a stably stratified environment is formed inside cavity during the injection, Worster and Hupper [3] extended the model of [2] to predict the density profile of the environment during the descent of the first front. The length, time and density are normalized respectively by

$$z = H\zeta, \quad t = t^*\tau, \quad g \frac{\rho - \rho_a}{\rho_a} = \frac{B_0^{2/3}}{4\alpha^{4/3}H^{5/3}}\delta \quad (2)$$

where $t^* = \frac{A}{4\pi^{2/3}\alpha^{4/3}H^{2/3}B_0^{1/3}}$, ρ is the mixture density, A is the cross-section and H is the height of the cavity, α is the entrainment coefficient and B_0 is the source buoyancy flux given by

$$B_0 = g \frac{\rho_a - \rho_i}{\rho_a} Q_0 \quad (3)$$

For a pure plume a value of 0.1 was taken in [2]. However, its value can vary down to 0.05 (see for examples [4], [5], [6], [7], [8], [9]). At constant temperature and pressure the volume fraction of the

injected fluid is calculated as

$$X = \frac{\rho_a - \rho}{\rho_a - \rho_i} \quad (4)$$

From this the normalized density is related to the volume fraction X by

$$X = X^*(-\delta) \quad (5)$$

where $X^* = \frac{B_0^{2/3}}{4\alpha^{4/3}H^{5/3}g^{\frac{\rho_a - \rho_i}{\rho_a}}}$. The normalized position of the first front ζ_0 and density δ are given respectively by

$$\zeta_0(\tau) = \left(1 + \frac{1}{5} \left(\frac{18}{5}\right)^{\frac{1}{3}} \tau\right)^{-\frac{3}{2}} \quad (6)$$

and

$$\delta(\zeta, \tau) = \frac{1 - \zeta^{\frac{5}{3}}}{1 - \zeta} 5 \left(\frac{5}{18}\right)^{\frac{1}{3}} \zeta^{-\frac{2}{3}} \left[1 - \frac{10}{39}\zeta - \frac{155}{8112}\zeta^2\right] - c(\tau) \quad (7)$$

where

$$c(\tau) = 5 \left(\frac{5}{18}\right)^{\frac{1}{3}} \left[\frac{\zeta_0^{-\frac{2}{3}} - 1}{1 - \zeta_0} + 3 \frac{1 - \zeta_0^{\frac{5}{3}}}{1 - \zeta_0} \left(\frac{1 - \zeta_0^{\frac{1}{3}}}{1 - \zeta_0} - \frac{5}{78} \frac{1 - \zeta_0^{\frac{4}{3}}}{1 - \zeta_0} - \frac{155}{56784} \frac{1 - \zeta_0^{\frac{7}{3}}}{1 - \zeta_0} \right) \right] \quad (8)$$

For more general situations, Cleaver et al. [6] proposed a volume Richardson number defined by

$$Ri_v = g \frac{\rho_a - \rho_i}{\rho_i} \frac{V^{1/3}}{U_0^2} \quad (9)$$

where V is the volume of the cavity. This number is a criterion to predict the build-up of concentration in an enclosed cavity. For high values of this number compared to unity, overturning does not occur and a stable stratification as predicted by the model of [2] applies. Otherwise, overturning occurs and near the ceiling a homogeneous layer is produced. In order to determine the limit of the homogeneous layer, Cariteau [4] conducted a set of experiments with helium-air mixture and helium in a parallelepiped cavity with a dimension of $H \times L \times W$. A tube of diameter d_i and height h_i is placed upward in the center of the bottom wall. The cavity is closed except for a small opening of diameter d_o in the middle of one side wall, at a height h_o from the floor, for depressurization. The cavity is initially filled with air at rest. Constant mass flux of helium is injected through the tube. During the experiment the temperature variation is negligible. Measurements of helium concentration is done by placing thermocouples (sensors) at 10 different heights along 2 vertical lines away from the source and are recorded in time. The experimental set-up and positions of those thermocouples are presented in Fig. 1.

Three filling regimes were found: stratified for $Ri_v > 3$, stratified with homogeneous layer and homogeneous for $Ri_v < 0.0032$. The stratified regime with 20 mm diameter source is in accordance with the model of [3], in which the entrainment coefficient α is from 0.04 to 0.065. However, the results for 5 mm diameter source contradicts this model and no satisfying explanation has been found.

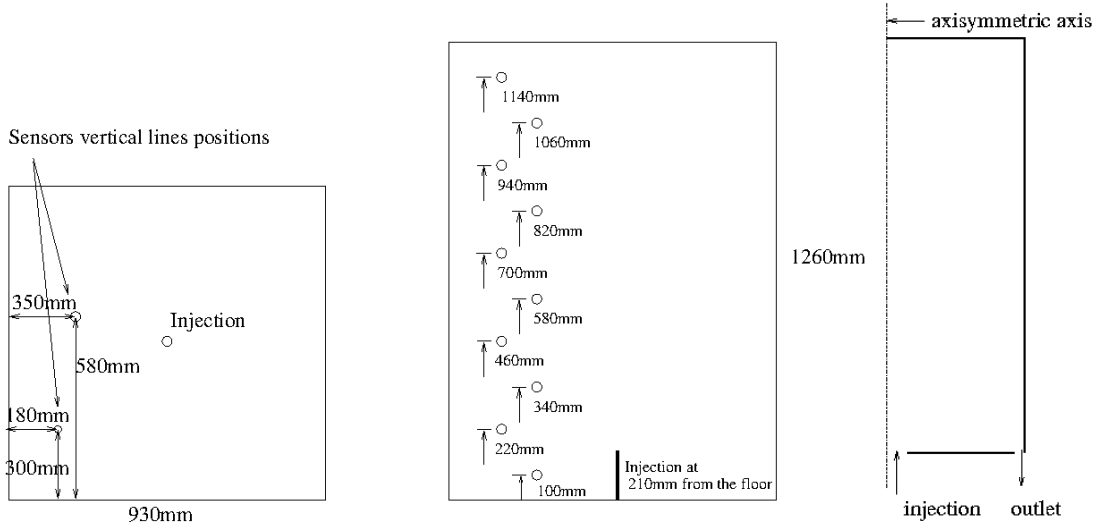


FIG. 1: The experimental set-up of the helium/air experiment : top view (left) and side view (center) and the computational domain (right). The thermocouples (sensors) are placed along two vertical lines. From bottom to top on outer line: thermocouples 6 to 10, on inner line: thermocouples 1 to 5.

III. PROBLEM MODEL AND NUMERICAL METHODS

In this section we present the configuration and the numerical methods for the numerical simulations.

A. Physical configuration

We consider the injection of helium in an air-filled cavity at constant temperature and pressure. The configuration is based on the experimental set-up of [11] whose results we want to reproduce. The experimental results [11] show that the helium volume fraction profiles are almost dependent only on the vertical position. Therefore, a cavity with the same horizontal section may produce the same results. We choose to mimic the experimental apparatus by a cylindrical cavity. The cross-sectional area A and the source diameter d_i are kept the same as in [11]. We only model the part of the cavity from the source exit so the new height L_z is equal to $H - h_i$. An opening is placed at the bottom and near the vertical side wall, which has $d_i/2$ the radial length. Only half of the domain is simulated. This configuration is called cavity 1 and is depicted in Fig. 1(right).

To begin with, four cavities with the same aspect ratio as cavity 1, from $1/10$ to $3/5$ of its size

H	L	W	d_i	h_i	d_o	h_o
0.126	0.93	0.93	0.02/0.005	0.21	0.01	0.01

TABLE I: Geometry parameters (in meter) of the helium/air experiment [4].

are simulated. Horizontal and vertical positions of sensors are also rescaled according to this size ratio. A flow rate Q_0 of 4 Nl/min (corresponding to $4.3 \cdot 10^{-3} m^3/s$) is used in accordance with the lowest injection flow rate of [11]. The corresponding injection Richardson number of 11.6 indicates that at the source the flow is dominated by buoyancy. In all the cases Sc_a is equal to 0.218. Other dimensionless parameters including the Grashof numbers, $Gr = g \frac{\rho_a - \rho_i}{\rho_a} \frac{L_z^3}{\nu_a^2}$, and the volume Richardson number, $Ri_v = g \frac{\rho_a - \rho_i}{\rho_i} \frac{V^{1/3}}{U_0^2}$, where ν is the kinematic viscosity of the ambient fluid, are given in table III.

The corresponding physical properties of helium and air are listed in table II. The binary diffusion coefficient of helium and air is calculated using the Chapman-Enskog's formula for non-polar molecules [13] and is only dependent on the temperature. The mixture physical properties (diffusion and viscosity) depends on the mass fraction of the components (see [12]) and are estimated at the same temperature as the experiment.

B. Governing equations

We make also a hypothesis that the flow is axisymmetric. We make use of the 2D axisymmetrical equations for the weakly compressible flow of a binary mixture. The equations are made dimensionless by the following reference quantities: the cavity height (L_z), the characteristic velocity used for natural convection flows ($\bar{U} = \sqrt{g \frac{\rho_a - \rho_i}{\rho_a} L_z}$), the ambient physical properties (ρ_a, ν_a) and the binary diffusion coefficient of helium and air (D). The resulting dimensionless set of equations

ρ_i	Y_i	ρ_a	Y_a	$\frac{\Delta\rho}{\rho_a}$	ν_i	ν_a	D
[kg/m ³]	[-]	[kg/m ³]	[-]	[-]	[m ² /s]	[m ² /s]	[m ² /s]
0.164	1	1.184	0	0.862	$11.7 \cdot 10^{-5}$	$1.51 \cdot 10^{-5}$	$6.93 \cdot 10^{-5}$

TABLE II: Physical properties of the test cases.

Cavity	Gr	d_i/d	Ri_v	Mesh	Time step
1/10	$4.3 \cdot 10^7$	0.19	1.05	50x98	10^{-4}
1/5	$3.4 \cdot 10^8$	0.1	8.4	98x194	10^{-4}
2/5	$2.7 \cdot 10^9$	0.05	67.2	194x386	10^{-4}
3/5	$9.3 \cdot 10^9$	0.03	226.8	290x578	10^{-4}

TABLE III: Dimensionless parameters of the simulated test cases.

are

$$\nabla \cdot \mathbf{u} = \frac{1}{ReSc_a}(\epsilon_M - 1)\nabla \cdot (\rho\nabla Y) \quad (10)$$

$$\frac{\partial \rho Y}{\partial t} + \nabla \cdot (\rho Y \mathbf{u}) = \frac{1}{ReSc_a} \nabla \cdot (\rho \nabla Y) \quad (11)$$

$$\frac{\partial \rho \mathbf{u}}{\partial t} + \nabla \cdot (\rho \mathbf{u} \otimes \mathbf{u}) = -\nabla p + \frac{1}{Re} \nabla \cdot (\rho \nu (\nabla \mathbf{u} + \nabla^t \mathbf{u})) + \frac{1}{Fr} \rho \mathbf{z} \quad (12)$$

$$\rho = \frac{1}{1 + (\epsilon_M - 1)Y} \quad (13)$$

where $\mathbf{u} = (u_r, u_z)$ stands for the velocity of the mixture, ρ the mixture density, Y the helium mass fraction and \mathbf{z} the unit vector oriented in the opposite direction to the gravity. The molar mass ratio of air to helium ϵ_M is equal to 7.24. The Reynolds Re and Froude Fr numbers are defined as: $Re = \frac{\bar{U}L_z}{\nu_a}$ and $Fr = \frac{\bar{U}^2}{gL_z}$. At constant temperature and pressure the helium mass fraction Y is related to the helium volume fraction X by

$$X = \frac{\epsilon_M Y}{1 + (\epsilon_M - 1)Y} \quad (14)$$

The boundary conditions are the following: at the bottom inlet ($r \leq d_i/2, z = 0$), a uniform profile is imposed for \mathbf{u} and Y corresponding to a volume flow rate of Q_0 and a total helium mass flux of $\rho_i Q_0$. At the bottom outlet, a Neumann boundary condition is applied for u_z and u_r is set to zero. u_z is then corrected to satisfy an integrating constraint on the velocity divergence. On the walls, a no-slip boundary condition is applied. The boundary condition for the helium mass fraction corresponds to a Neumann boundary condition for Y ($\partial Y / \partial z = 0$) applied on all walls and at the bottom outlet.

C. Numerical methods

Equations (10-13) are solved in the axisymmetrical coordinates using a second-order semi-implicit scheme. It combines a second-order backward differential formula (BDF2) with an implicit treatment for the diffusion terms and an explicit second-order Adams-Bashforth extrapolation for the nonlinear terms. The coupling between the velocity and the dynamic pressure is handled by a projection method which retains second-order accuracy of the time integration. A finite-volume discretization on a staggered grid is used. Second-order central difference scheme is employed for all the spatial derivative terms. The discrete systems resulting from the finite-volume approach are split by an ADI technique and then solved by Thomas algorithm, while the Poisson-like equation for the pressure correction is solved by a multigrid method.

Our numerical methods have been used to simulate a buoyant jet of glycerol-water [14] in a tank and the numerical results are in excellent agreement with the experimental results.

A uniform grid has been used in both x and z -direction. The mesh size and the non-dimensional time step at the beginning of the computation of each case is given in Table III. Later the time

step is doubled to speed up the calculation. However, it has to respect a constraint on the CFL number for the calculation to be stable.

At the present time the grid convergence has been done for cavity 1/10 with 50x98 and 98x194 grids. Comparison in Fig. 2 shows minor differences of the solutions between two grids.

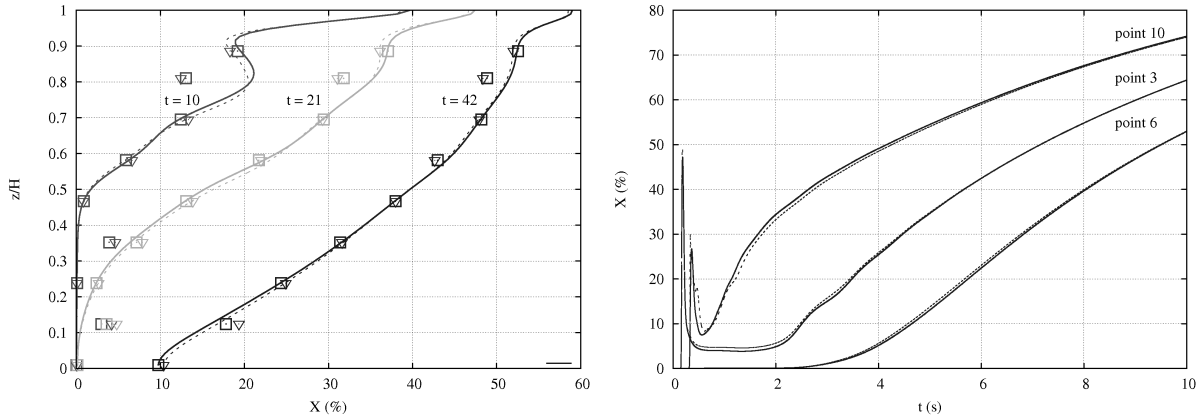


FIG. 2: Helium volume fraction for cavity 1/10 with 50x98 grid (solid curves, \square) and 98x194 grid (dashed curves, ∇). Left: helium volume fraction profile along the outer line going through sensors 6 to 10, right: time evolution of helium volume fraction at 3 sensors 3, 6 and 10.

IV. RESULTS

In this section we present the numerical results for the four cavities. The flow structure is presented first and followed by a comparison with the model of [3]. Cariteau [4] has shown that though the experimental set-up of [11] does not satisfy the condition $H/d \leq 0.5$, the results of [11] can be compared satisfactorily to the model of [3].

The vorticity fields for cavity 3/5 in Fig. 3 show the evolution of the flow in time. The computational results are reflected through the vertical axis to obtain the whole field. It is shown that the plume carrying two stable vortices impact the top wall and spreads out horizontally to form a thin layer. This layer propagates downward due to the entrainment of the new injected fluid and the fluid above it becomes stably stratified. Motion is visible in the core region of the plume and at the top wall where the fluid is continuously entrained by the new fluid. In other regions everything is almost steady.

The snapshots of the volume fraction fields are shown in Fig. 4 for cavities from 1/10 to 3/5. It is shown that in the regions near the axis and near the top wall, helium volume fraction profile is affected by the developing plume. In the remaining region the helium volume fraction profile is nearly one-dimensional. Cavity 1/10 is relatively small, so helium volume fraction is not really 1-dimensional. When the size of the cavity is increased we have nearly one-dimensional profile in the region between the plume axis and the vertical wall.

Helium volume fraction profile during the descent of the first front

We compare the normalized helium volume fraction profile during the descending of the first front

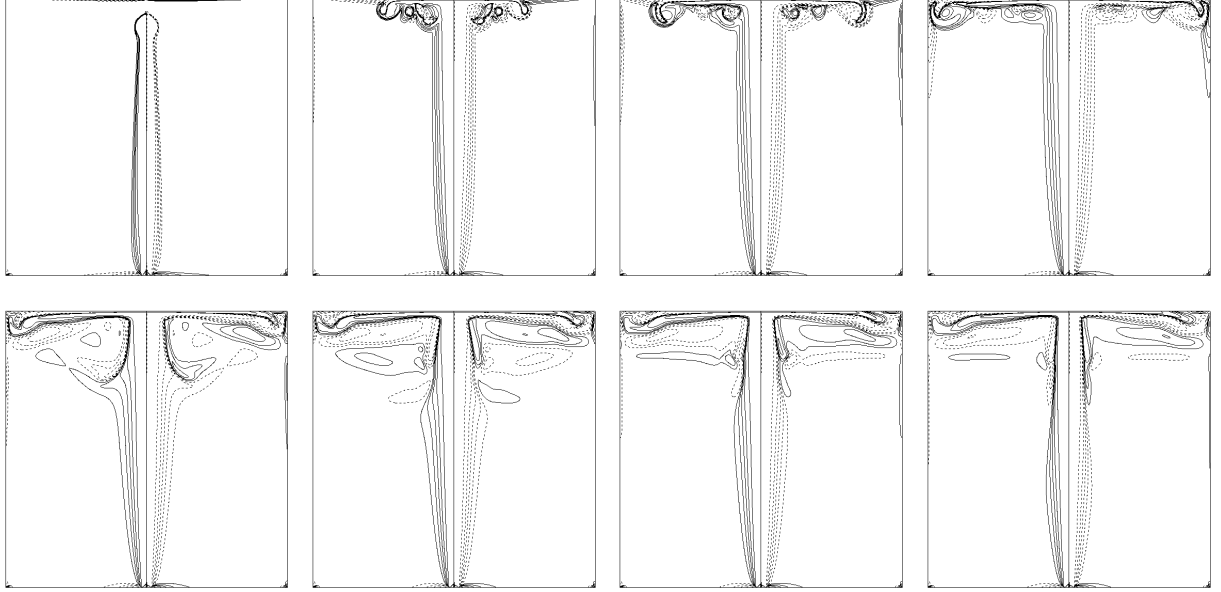


FIG. 3: Vorticity isocontour respectively at $t=4, 10, 20, 46, 93, 139$ and 260 for cavity $3/5$ (from left to right, top to bottom).

with the model of [3] in Fig. 5. The time and helium volume fraction are normalized using Eqs. (2) and (5), respectively, and the normalized helium volume fraction is compared with $\delta(\zeta, \tau)$ in Eq. (7). Solid curves represent the helium volume fraction along the outer line passing through sensors 6 to 10. Some points are not on any curves since the helium fraction profile is not exactly one-dimensional in the cavity. This happens for the smallest cavity in which the sensors are placed too close to the axis and is hence directly affected by the instability of the developing plume. This also happens for larger cavities at early times due to the instability in establishing the first front. However, when the front is well established all the points collapse on the corresponding curves. The entrainment coefficient in the normalization scheme was adjusted to give a reasonable fit of the data. It is decreasing from $\alpha = 0.17$ to $\alpha = 0.04$ for cavity $1/10$ to $3/5$. In the model of Worster and Huppert [3] the entrainment coefficient α is supposed to be independent of the distance from the source and is taken equal to 0.1. A review of literature in [4] shows that α vary from 0.05 to 0.1 for pure jets to pure plumes. Cariteau, in the comparison of experimental results [4] and the model [3], used α from 0.04 to 0.065. Our adjustment here is somewhat exceeding this limit. On the other hand, the trend of adjusting the entrainment coefficient α seems to contradict the literature. For cavity $1/10$, the top wall is not far from the source and the buoyant jet behaves like a jet. However, $\alpha = 0.17$ is higher compared to $\alpha = 0.1$ normally taken for pure plumes in the literature. For cavity $3/5$, the top wall is far from the source and the buoyant jet behaves like a plume. However, $\alpha = 0.04$ is smaller compared to $\alpha = 0.05$ normally taken for pure jets in the literature. We have not been able to explain this contradiction. Another observation is that even with the adjustment of the entrainment coefficient α , the numerical results do not seem to collapse on the theoretical curves. The profiles obtained in the numerical results are closer to linear. Our hypothesis of axisymmetric flow may be the key point of this behavior. The linearity seems increasing for increasing size of the cavity may be affected by the increasing ratio of cavity radius to injection radius $\frac{d}{d_i}$. Cariteau [4] also observed this linearity behavior in his experiment with 5 mm diameter source, while with 20 mm diameter source the solution is close to the model of [3].

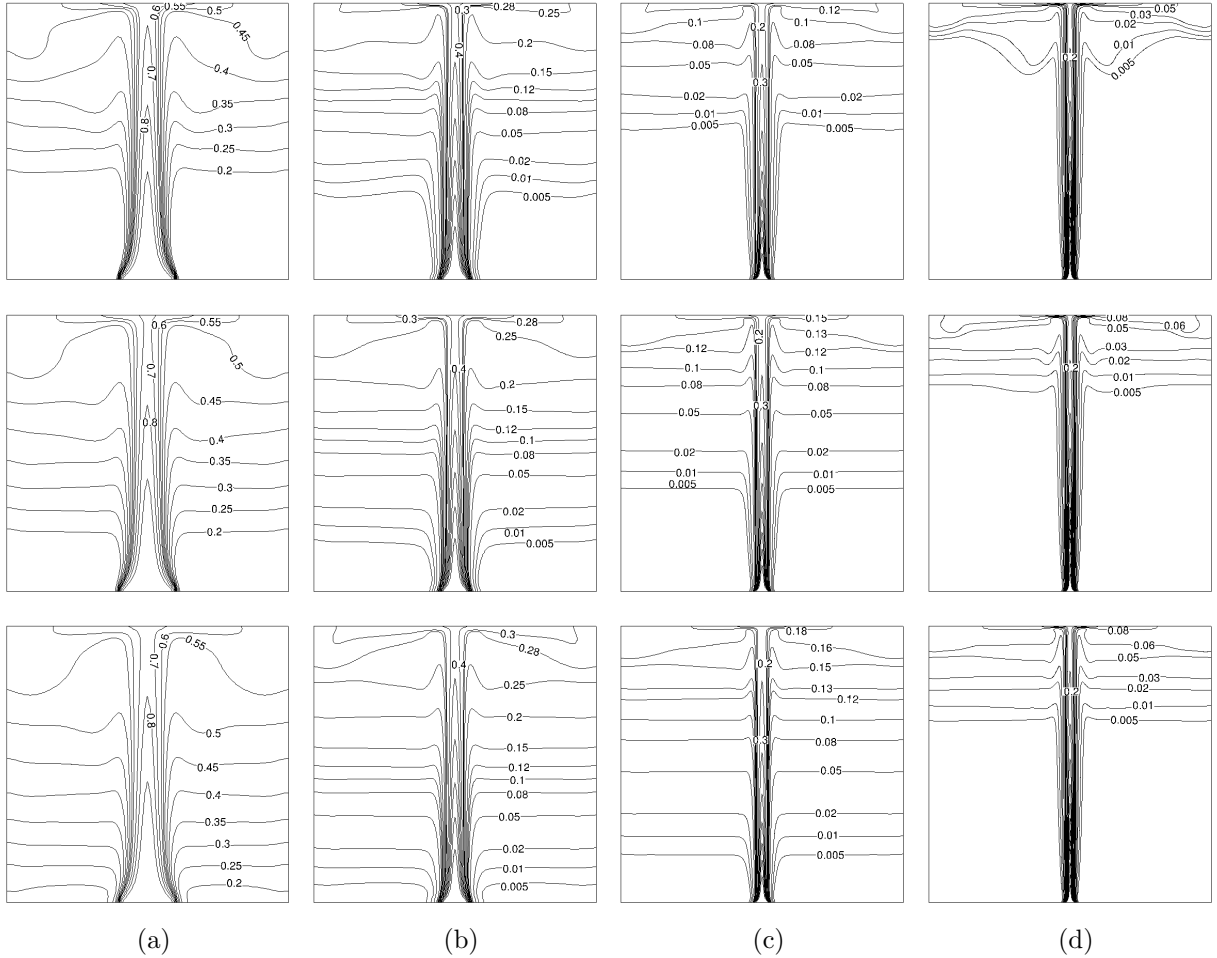


FIG. 4: Helium volume fraction fields: a) Cavity 1/10 at $t= 32, 42$ and 53 ; b) Cavity 1/5 at $t= 56, 75$ and 94 ; c) Cavity 2/5 at $t= 100, 164$ and 264 ; d) Cavity 3/5 at $t= 46, 93$ and 139 (from top to bottom).

V. DISCUSSIONS AND CONCLUDING REMARKS

We have developed a numerical tool to simulate the mixing and dispersion of helium injected in an air-filled cavity. The final goal is to reproduce the benchmark experimental results of [11]. We made an assumption of axisymmetric flow to reduce the dimension of the problem. To begin with, four cavities with the same aspect ratio and injection condition as the experimental set-up [11] but different size are investigated. The numerical results show almost one-dimensional profile of the helium volume fraction in the cavity, as found in the experimental results of [11]. The vertical helium volume fraction profiles during the descent of the initial front are compared with the model of [3]. The entrainment coefficient has to be adjusted from 0.17 to 0.04. It is larger for smaller cavities and smaller for larger cavities. This seems to contradict the literature since near the source the buoyant jet behaves like a jet and α should be small, while far from the source the buoyant jet behaves like a plume and α should be larger. With the chosen α the fit with the model is not very good since the numerical profiles show a strong linearity which is not observed in the model of [3]. However it was observed in experimental results of [4] for the 5mm-diameter source. This

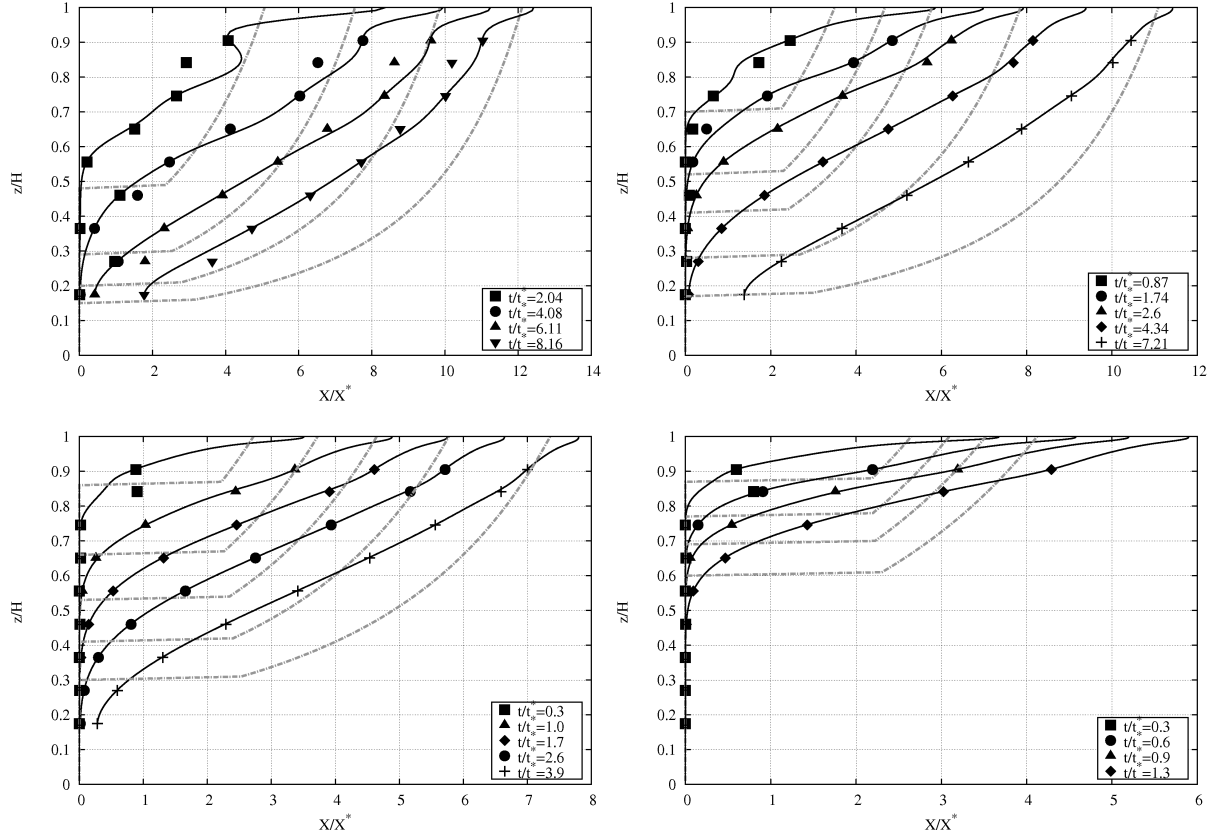


FIG. 5: Normalized helium volume fraction variation with height, from top to bottom, left to right: cavity 1/10, $\alpha = 0.17$; cavity 1/5, $\alpha = 0.09$; cavity 2/5, $\alpha = 0.045$; cavity 3/5, $\alpha = 0.04$. Symbols represent for sensors from 2 to 10, solid curves for outer vertical lines passing through sensors 6 to 10 and dashed curves for model of Worster and Huppert [3]

linearity may be due to the axisymmetric hypothesis we have made. However, further investigation is needed to understand the trend of adjustment of the entrainment coefficient in our study.

-
- [1] C. J. Chen and W. Rodi 1980 A Review of Experimental Data. *Pergamon Press*
 - [2] W. D. Baines and J. S. Turner 1969 Turbulent buoyant convection from a source in confined region. *J. Fluid Mech.* **37(1)** 51-80
 - [3] M. G. Worster and H. E. Huppert 1983 Time-dependent density profiles in a filling box. *J. Fluid Mech.* **132**
 - [4] B. Cariteau and I. Tkatschenko 2012 Experimental study of the concentration build-up regimes in an enclosure without ventilation. *International Journal of Hydrogen Energy* **37**
 - [5] P. N. Papanikolaou and E. J. List 1988 Investigation of round vertical turbulent buoyant jets. *J. Fluid Mech.* **195** 341-91
 - [6] R. P. Cleaver and M. R. Marshall and P. F. Linden 1994 The build-up of concentration within a single enclosed volume following a release of natural gas. *J. Hazard. Mater.* **36** 209-226
 - [7] A. E. Germeles 1975 Forced plumes and mixing of liquids in tanks. *J. Fluid Mech.* **71** 601-623
 - [8] B. J. Lowesmith and G. Hankinson and C. Spataru and M. Stobbart 2009 Gas build-up in a domestic property following releases of methane/hydrogen mixture. *Int. J. Hydrogen Energy* **34** 5902-5911

- [9] A. G. Venetsanos and E. Papanikolaou and B. Cariteau and P. Adams and A. Bengaouer 2010 Hydrogen permeation from CGH2 vehicles in garages: CFD dispersion calculations and experimental validation. *Int. J. Hydrogen Energy* **35** 3848-3856
- [10] M. R. Swain and P. Filoso and E. S. Grilliot and M. N. Swain 2003 Hydrogen leakage into simple geometric enclosures. *Int. J. Hydrogen Energy* **28** 229-248
- [11] G. Bernard-Michel and J. Trochon and E. Vyazmina and O. Gentilhomme 2012 Resultat du benchmark ventilation sur 3 essais GAMELAN dans le cadre du projet ANR DIMITRHY. *CEA Saclay DEN/DANS/DM2S/STMF/LIEFT DEN/DANS/DM2S/STMF/LIEFT/RT/12/020/A*
- [12] C. R. Wilke 1950 A viscosity equation for gas mixture. *The Journal of Chemical Physics* **18**
- [13] R. B. Bird and W. E. Stewart and E. N. Lightfoot 2001 Transport phenomena. *John Wiley & Sons*
- [14] M. C. Rogers and S. W. Morris 2009 Natural versus forced convection in laminar starting plumes. *Physics of Fluids* **21**